ELSEVIER

Physics of the Earth and Planetary Interiors 120 (2000) 271–287

PHYSICS OF THE EARTH AND PLANETARY INTERIORS

www.elsevier.com/locate/pepi

Reversal sequence in a multiple scale dynamo mechanism

C. Narteau [a,*], E. Blanter [a,b], J.-L. Le Mouël [a], M. Shirnman [a,b], C.J. Allègre [a,c]

[a] *Institut de Physique du Globe de Paris, 4, Place Jussieu, Paris, Cedex 05, 75252, France*

[b] *International Institute of Earthquake Prediction Theory and Mathematical Geophysics, Warshavskoye shosse, 79, korp 2, Moscow 113556, Russia*

[c] *Université Paris VII, 4, Place Jussieu, 75252 Paris Cedex 05, France*

Received 30 November 1999; accepted 25 February 2000

Abstract

We investigate the temporal evolution of the magnetic dipole field intensity of the Earth through a multiscale dynamo mechanism. On a large range of spatio-temporal scales, the helical motions of the fluid flow are given by a schematic model of a fully developed turbulence. The system construction is symmetric with respect to left-handed and right-handed cyclones. The multiscale cyclonic turbulence coupled with a differential rotation (schematic $\alpha\omega$ dynamo) or alone (schematic α^2 dynamo) is the ingredient of the loop through which poloidal and toroidal fields are built from one another. Two kinds of reaction of the magnetic field on the flow are considered: the presence of a magnetic field first favours a larger-scale organization of the flow, and, second, impedes this flow by the effect of growing Lorentz forces. We obtain the general features of the geomagnetic field intensity observed over geological times and describe a general mechanism for reversals, excursions and secular variation. The mechanism happens to keep a memory during the chrons and loose it during the events (excursions and inversions). © 2000 Elsevier Science B.V. All rights reserved.

Keywords: Geomagnetism; Dynamo; Hierarchical system; Cascade; Reversal and excursion

1. Introduction

The present-day magnetic field of the Earth, as measured at the Earth's surface or aboard low altitude satellites, appears to be grossly the field of a magnetic dipole located at the Earth's center and inclined by 11° on the rotation axis. When taken on the average over a few thousands of years, the geomagnetic field is the field of a centered axial dipole, i.e. aligned along the rotation axis. When considering longer time spans, millions to hundreds of millions of years, it comes out that the polarity of this (equivalent) axial dipole frequently changes with time, going from North–South to South–North and conversely; these are the so-called reversals of the geomagnetic field. Periods between reversals are called polarity intervals, or chrons. The average duration of the polarity intervals has changed over geological times from about 1 Ma (1 million years) 80 Ma ago to 0.2 Ma today. The duration of the reversals (typically 4 or 5 ka (thousands of years)) is short compared to the duration of the chrons. Sometimes, very long polarity intervals (superchrons) occur, e.g. the Cretaceous superchron, which extends

* Corresponding author. Tel.: +33-1-44-27-38-10; fax: +33-1-44-27-24-87.

E-mail address: narteau@ipgp.jussieu.fr (C. Narteau).

0031-9201/00/$ - see front matter © 2000 Elsevier Science B.V. All rights reserved.
PII: S0031-9201(00)00145-X

from 118 to 83 Ma before the present time. During a chron, the intensity of the dipole fluctuates. From time to time, large decreases of the dipolar field accompanied by large changes in the field direction, and intensity at the Earth's surface — it is no longer the field of an axial centered dipole — occur, which do not lead to a reversal; these are the so-called excursions. Fig. 1 shows the behavior of the paleomagnetic field over the last 4 Ma. The present paper is devoted to the behavior of the geomagnetic field over geological times, i.e. to the reversals and the succession of polarity intervals.

It is now generally accepted that the Earth's magnetic field is generated by a dynamo operating in the outer liquid core of the planet. A considerable amount of work as been devoted to dynamo theory. Impressive numerical codes have been recently built, which numerically solve the magnetohydrodynamic equations and have given spectacular results (Glatzmaier and Roberts, 1995a; Kuang and Bloxham, 1997; Kageyama and Sato, 1997). In particular, reversals are obtained in these numerical models (Glatzmaier and Roberts, 1995b), although their mechanism and meaning are not yet well understood. Nevertheless, these computations, however heavy, cannot be performed for realistic values of the parameters involved, in particular the viscosity (only Ekman number values not smaller than 10^{-6} can be used in the models, whereas this value is probably 10^{-15} for the real Earth).

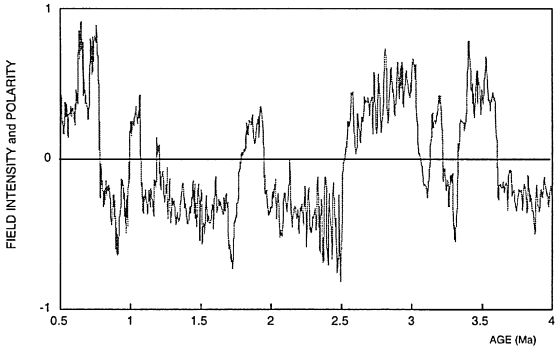

Fig. 1. Relative variations of the dipole field intensity during the past 4 Ma after multiplying by -1 the intensities associated with a reverse directio (from Valet and Meynadier, 1993). Note the the orientation of time on the abscissae axis.

Before these numerical codes existed, an intermediate approach was to consider parametrical models such as the $\alpha\omega$ or α^2 geodynamo models (e.g. Krause and Rädler, 1980; Moffatt, 1978; Roberts, 1971; Gubbins, 1974; Braginsky, 1978; Braginsky and Roberts, 1987). In α^2 dynamos, a small scale turbulent motion, nonmirror-symmetric, was supposed to exist in the core, with, in general, a mean helicity having different signs in the Northern and Southern hemispheres (α effect; see infra). In $\alpha\omega$ dynamos, in addition to this turbulent motion, a differential rotation of the core layers (ω effect) was supposed to exist.

In two former papers, Le Mouël et al. (1997) and Blanter et al. (1999), we considered what we called a multiscale dynamo with, as an ingredient, instead of a small-scale turbulence, a fully developed one, or rather a schematic model of developed turbulence in the form of a multiscale helical motion. In Le Mouël et al. (1997) ((I) from now on), this ingredient was used together with a differential rotation to construct some kind of an abstract $\alpha\omega$ dynamo. In Blanter et al. (1999) ((II) from now on), the turbulence was modeled along somewhat different lines; it was shown that long-lived spontaneous symmetry breakings — polarity intervals — were obtained as soon as up and down cascades were both taking place in the turbulent flow. But the dynamo mechanism investigated was not an auto-excited one since a preexisting magnetic field — which, however, could be small — was assumed. In the present work, we introduce the multiscale helical motion of (II) into the formalism of (I) in order to build a model closer to an auto-excited dynamo model, although still rather abstract and schematic. It was announced in (II) that this new model would exhibit features coming from the two first ones.

Trying to catch the gross features of the behaviour of this highly complex geodynamo through quite simplified models is a time-honoured approach. Among them, considering a small number of well-chosen differential equations — a method that has been credited of success in other fields of physics and geophysics — has received much attention. Without trying to give here any exhaustive list of these tentatives, we will only quote the seminal papers of Bullard and Gellman (1954), Rikitake (1958), Nozières (1978) and Hide (1998). In this

latter example, relative again to the disk dynamo, it is shown that a complete quenching of current fluctuations in a self-exciting homopolar dynamo is possible, and the role of changing boundary conditions in the geodynamo problem is reassessed (see Section 7).

We will consider two different kinds of models, with different symmetries, which we will call somewhat loosely $\alpha\omega$ and α^2 models. We will describe the behaviour and effect of the helical flow mechanism in some detail for the case of the first model. We will then present more briefly the second one.

2. Schematic equations of a $\alpha\omega$ dynamo

As announced above, we will consider in the following a formal simplified description of a dynamo. Let us decompose the magnetic field, $\vec{B}$, into a poloidal, $\vec{B}_S$, and a toroidal, $\vec{B}_T$, components (e.g. Backus (1958)):

$$\vec{B} = \vec{B}_S + \vec{B}_T. \quad (1)$$

In addition, we suppose that each of the components, $\vec{B}_S$ and $\vec{B}_T$, can be written in the form of the product of a space function by a time function (see (I)):

$$\vec{B}_T(\vec{r},t) = T(t)\vec{\mathscr{B}}_T(\vec{r}), \quad (2)$$

$$\vec{B}_S(\vec{r},t) = S(t)\vec{\mathscr{B}}_S(\vec{r}). \quad (3)$$

In other words, we consider a single mode of both the toroidal and the poloidal fields. For example, $\vec{\mathscr{B}}_S(\vec{r})$ could be the poloidal mode $\vec{P}_1^0$ and $\vec{\mathscr{B}}_T(\vec{r})$ could be the toroidal mode $\vec{T}_2^0$.

As in (I), we first suppose that the toroidal field is generated from the poloidal one through differential rotation, while the poloidal field is generated from the toroidal one from the multiscale helical motion (see below). Therefore, our working equations will be:

$$\frac{\partial T}{\partial t} + K_T T = \omega S, \quad (4)$$

$$\frac{\partial S}{\partial t} + K_S S = \Delta p\zeta_T T, \quad (5)$$

ωS is the toroidal source term (for the considered mode) due to the differential rotation; $\Delta p\zeta_T T$ is the poloidal source term (for the considered mode) due to the interaction of our multiscale helical motion with the toroidal field; it will be explained explicitly below. $K_S S$ and $K_T T$ are diffusive terms, K_S^{-1} and K_T^{-1} the diffusive times for the poloidal and toroidal fields (modes), respectively. We will call the model ruled by Eqs. 4 and 5 an $\alpha\omega$ dynamo, although it is of course rather different from classical $\alpha\omega$ models.

We will afterwards consider a more symmetrical mechanism (Section 6) in which the source term for both the poloidal and the toroidal fields results from the interaction of the helical multiscale motion with these fields; this model — with the same reservations as above — will be called an α^2 dynamo.

One can also consider Eqs. 4 and 5, with $\Delta p\zeta_T$ defined in the next section, and their solutions $S(t)$ and $T(t)$ for themselves, as an illustration of an original dynamical system.

3. The multiscale helical flow model

The model of helical flow is given in full detail in (II). We have not significantly modified it in the present paper, except for the expression of the source term of magnetic field and for the introduction of a retroaction of the magnetic field on the flow; therefore, we will here limit ourselves to a summarized description of this part of the model.

The hierarchical system represents a given volume of conducting fluid. Scaling properties of the turbulence govern the hierarchical construction of the model. Helical vortices or cyclones (Fig. 2(a)) of different scales appear in hierarchically organized cells (Fig. 2(b)). Interactions between cyclones exist, which are mainly due to electromagnetic forces. The helical vortices can be left-handed or right-handed, say have two orientations, 1 and 2. The interaction of the cyclones with a prevailing toroidal magnetic field generates a secondary magnetic field, which contributes to the poloidal mode $\vec{\mathscr{B}}_S(\vec{r})$, adding an increment to $S(t)$ (and, conversely, exchanging poloidal and toroidal, in Section 6). Globally, the intensity and sign of the source term (r.h.s. member of Eq. (5)) depend on the number, scales and orientations (1 or 2) of the cyclones involved in the turbulent motion at the time considered. The expression of $\Delta p\zeta_T$ will be given below, after defining strong and weak cyclones.

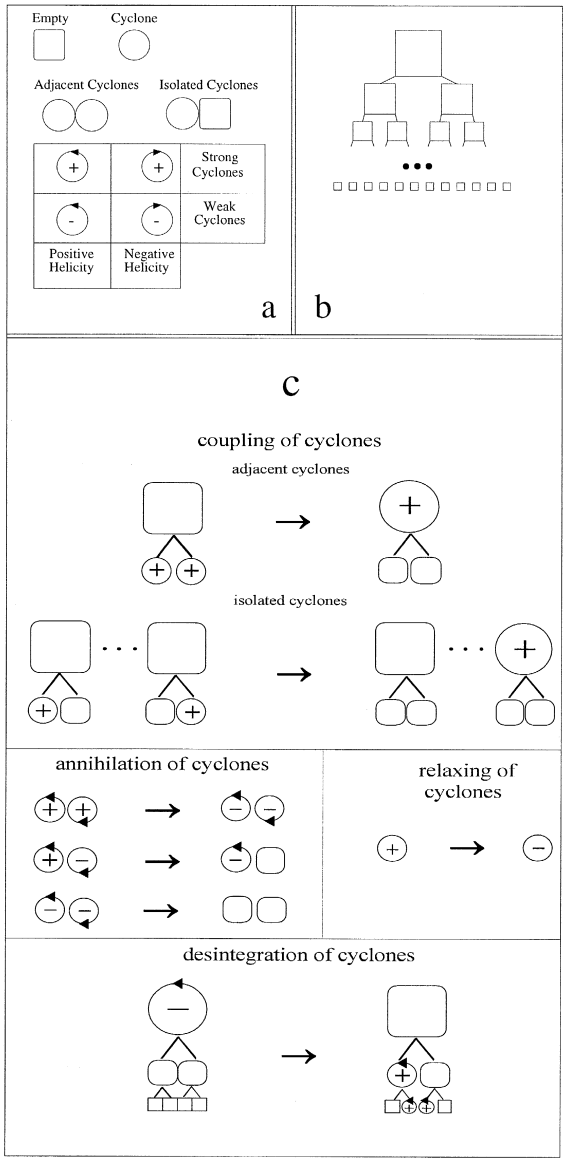

Fig. 2. (a) Different posible states for a given cell; (b) hierarchical structure of our model; (c) all the possible transitions: coupling of cyclones generates an inverse cascade; desintegration of cyclones generates a direct cascade.

The turbulence generates cyclones of both orientations; a mirror symmetry of the turbulence generation is postulated: cyclones of orientation 1 and cyclones of orientation 2 appear with the same probability; the evolution of cyclones of both orientations is also ruled by the same parameters. Despite this symmetry in the generation of turbulence, spontaneous symmetry breakings may occur, leading to large-scale lacks of mirror symmetry. As in (II), the efficiency of the turbulence is characterized at all scales by

$$\mathcal{T}(l) = E_0 \epsilon^l, \qquad \epsilon < 1, \tag{6}$$

where E_0 is the parameter of turbulence and ϵ is a scaling parameter.

The turbulence sustains the existence of cyclones during a random time interval; the temporal evolution of a cyclone is governed by a continuously increasing instability, which eventually leads to its destruction. The increase of a cyclone instability can be viewed as a relaxing process in the course of which the cyclones properties change continuously. For the sake of simplicity, we introduce a discretisation of the relaxing process: two living states of the cyclones (weak or strong) are considered (Fig. 2). The strong state is characteristic of a cyclone soon after its appearance; the weak state is characteristic of a cyclone before its destruction. The characteristic size of a cyclone is kept constant, but its configuration is supposed to evolve through its interaction with the magnetic field. Quantitatively, a strong (or [+]) cyclone of level l transforms into a weak (or [−]) cyclone with a transition rate $D(l)$ (Fig. 2(c)). This transition rate does not depend on the orientation of the cyclone and does not change in time. It is expressed as follows:

$$D(l) = D_0 \delta^l, \qquad \delta < 1, \tag{7}$$

where D_0 is the parameter of relaxing and δ is a scaling parameter. The scaling relationship between the relaxing transition rate $D(l)$ and the level l accounts for the property of cyclones of high levels to keep longer their strong state; the relaxing transition rate $D(l)$ is indeed inversely proportional to the average lifetime of the [+] cyclone of level l.

Weak cyclones can be randomly disintegrated at each point in time. Disintegration of weak cyclones of level l into cyclones of lower levels results in the disappearing of [−] cyclones at level l and appearance of new cyclones with the same orientation at all levels smaller than l (Fig. 2(c)). Weak cyclones of level l disappear with a transition rate $\beta(l)$ invariant in time and independent of the cyclones orientation:

$$\beta(l) = \beta_0 b^l, \qquad b < 1, \tag{8}$$

where β_0 is the parameter of disintegration and b is a scaling parameter. The lifetime of weak cyclones is inversely proportionnal to the disappearing transition rate β. Larger-scale cyclones have a longer lifetime. Disintegration of $[-]$ cyclones at level l and appearance at time t of new cyclones of all levels lower than l make the direct cascade of appearance of new cyclones whose flow expression is given in (II). The efficiency of the direct cascade is characterized by a parameter F_0 (II).

Interactions between cyclones are governed by attraction (repulsion) of parallel (antiparallel) electric currents generated by these cyclones in the magnetic field. Adjacent or isolated strong cyclones of level l (Fig. 2(c)) may be coupled if they have the same orientation. The coupling of cyclones leads to a transition from level l to level $(l+1)$: the two coupled cyclones of level l disappear at this level, and a new cyclone of the same orientation appears at level $(l+1)$. Coupling transition rates $\alpha(l)$ for adjacent cyclones or $\gamma(l)$ for isolated cyclones are invariant in time, do not depend on the orientation 1 or 2 of the coupling cyclones, and decrease with the level as follows:

$$\alpha(l) = \alpha_0 \mu^l, \qquad \mu < 1, \tag{9}$$

$$\gamma(l) = \gamma_0 g^l, \qquad g < 1, \tag{10}$$

where α_0 and γ_0 are respectively the coupling parameters of adjacent and isolated cyclones and μ and g are scaling parameters. This is the inverse cascade of appearance of new cyclones.

For computational reasons, it is assumed that all the processes described above take place in time during one time step δt of the modeling (for the same reason, the differential equations, Eqs. 4 and 5, are replaced by their finite difference approximation with δt as time step). Let us recapitulate the way the cyclones appear and disappear in the model, generating a continuously evolving turbulence.

3.1. Appearance of new cyclones

There are three different causes of apparition of new cyclones at a given level l (see Fig. 2):

- the turbulence generates continuously new cyclones at all levels of the system (Eq. (6)) in equal numbers for both orientations (mirror symmetry of the generation mechanism).
- two strong cyclones of level l can couple to give a new strong cyclone of level $(l+1)$. Globally, this coupling process produces an inverse cascade from lower to higher levels of the system.
- weak cyclones of level l, which have disintegrated at time $(t-\delta t)$, contribute to the appearance of new cyclones at all levels lower than l at time t. Globally, the disintegration process produces a direct cascade from higher to lower levels of the system.

3.2. Disappearance of cyclones

There are three different ways for cyclones to disappear at a given level l (see Fig. 2). These processes are not independent from the appearance ones:

- disintegration of weak cyclones. New cyclones appear at lower levels at the next time moment (vide supra).
- coupling of strong cyclones of level l leads to the disappearance of the coupling cyclones at level l (and to the appearance of new cyclones at the higher level; vide supra).
- annihilation of a weak cyclone with an adjacent one of the opposite orientation. No new cyclone appears in this case (Fig. 2).

The time sequence of the different steps of the flow evolution enumerated above is detailed in (II), together with explicative drawings.

4. The retroaction of the magnetic field

As pointed out above, the change brought to the flow model of (II) is the introduction of a retroaction of the magnetic field (in addition to the electromagnetic coupling leading to the inverse cascade).

Two kinds of reaction of the magnetic field on the flow will be considered. First, we will assume that the presence of a magnetic field favours a larger-scale organization of the flow, i.e. favours larger-range

eddies at the expense of lower-range ones (see points A below). After the pioneering work of Chandrasekar (1961), such an effect was suggested by Frisch et al. (1975) in the case of a magnetohydrodynamic turbulence. Three-dimensional numerical simulations of injection of small-scale turbulence with helicity have confirmed that an inverse cascade occurs leading to an increase of the magnetic field and of the flow at larger spatial scales (Pouquet and Patterson, 1978; Meneguzzi et al., 1981). In geophysics, such an effect has also been obtained in numerical simulations (Cardin and Olson, 1995) and experiments (Brito et al., 1995). Second, as in any dynamo model, some mechanism must prevent the magnetic field from increasing indefinitely (points B below); the flow is impeded by the growing Lorentz forces.

In the present abstract model, these two effects are taken into account in the following way:

(A) The coupling of strong cyclones is favoured by the magnetic field, i.e. increases when the field increases, whereas the disintegration of weak cyclones is made more difficult for higher ranges when the field is larger.
(B) The transformation of strong cyclones into weak cyclones is favoured by the magnetic field, i.e. increases when the field increases, and, simultaneously, cyclones evolve towards a new configuration, which generates less secondary magnetic field.

Practically, after defining a magnetic energy

$$W = S^2 + T^2,$$

we suppose that the following are true.

(A.1) The transition rate of coupling of strong cyclones (Eqs. 9 and 10) increases with W:

$$\alpha(l) = \alpha_0(1 + \lambda W)\,\mu^l, \tag{11}$$

$$\gamma(l) = \gamma_0(1 + \lambda W)\,g^l. \tag{12}$$

(A.2) The disintegration of weak cyclones of degree l into cyclones of lower levels giving rise to the direct cascade is slowed by the magnetic field. In formula 8:

$$b = b_0 \exp(-\nu W). \tag{13}$$

The ratio of lifetimes of small-degree cyclones to lifetimes of high-degree cyclones decreases when the amplitude of the magnetic field increases.

(B.1) As for the saturation mechanism, we simply assume that the transition rate of relaxation of strong [+] cyclones, i.e. the probability per unit of time for a strong cyclone of level l to transform into a weak [−] inefficient cyclone of the same level (Eq. (1) in (II)) increases with W. In formula 8:

$$D(l) = D_0(1 + \kappa W)\,\delta^l. \tag{14}$$

(B.2) The expression of the source term in (5), i.e. of $\Delta p \zeta T$, is modified with respect to the corresponding expression in (II). Here, indeed we consider that the weak [−] cyclones are much less efficient in generating the magnetic fields than the strong ones. Physically, this means that, in addition to becoming less energetic with time (which leads to the transformation of strong cyclones into weak cyclones in our schematic two steps evolution), the cyclones also tend to transform their configuration in such a way as to become less efficient in building new fields by interacting with the existing fields; this evolution can be seen as an effect of Lenz law. So, formula (11) of (II) is replaced by:

$$\Delta p \zeta_T = \zeta_T \sum_{l=1}^{L} \left(\left(p_1^+(l,t) - p_2^+(l,t) \right) + \rho\left(p_1^-(l,t) - p_2^-(l,t) \right) \right) \chi^l, \tag{15}$$

with $0 < \rho \ll 1$. ζ_T, which has the dimension of inverse of time, characterizes the global efficiency of turbulence. $p_i^{\pm}(l,t)$ denotes the ratio of cyclones of ith orientation, in state [+] or [−], at level l, at time t, to the total number of cells (we will call this ratio density).

In fact, as will appear in what follows, although the helical flow model of (II) is kept essentially unchanged, except for the retroaction of the magnetic field, the polarity intervals and reversals are obtained here in a different way. In (II), indeed, the secondary magnetic field generated by the turbulent flow in a primary magnetic field H_0 was considered to be $H_0 \Delta p$, and the process was stopped there. Here, the quantity $\Delta p \zeta_T T$ is a source term of poloidal field entering the r.h.s. member of the differential Eq. (5).

5. Realisations of an $\alpha\omega$ dynamo

Let us start with a remark; for the model to lead to polarity intervals during which S and T fluctuate around more or less stationary values S_0, T_0, with the choice of signs made in Eq. (15), we must have $\zeta_T \Delta p \omega > 0$, i.e. roughly speaking, a domination of cyclones of orientation 1 since ζ_T and ω are chosen > 0; on the contrary, as will be seen in Section 5.2, time spans when $\Delta p < 0$ are time spans during which the field (S_0, T_0) can be destabilized.

We will now present the results of a numerical experiment; parameters values are given in Table 1. As in (II), we give a common value to groups of parameters (Table 1 of (II)). The obtained realisation is typical of a large domain of parameters. In our numerical simulations, the time step can be calibrated from the values given to the diffusion times K_S^{-1} and K_T^{-1}. It is of the order of 1 year if $K_S^{-1} \sim K_T^{-1} \sim 10^4$ years. In the following, we will often express times in years following this convention. Note that all the transition rates are quantitatively defined from the values of these diffusion times.

Fig. 3 represents the evolution of $S(t)$ and $T(t)$ over a time span of 2.5×10^7 years. Polarity intervals (chrons), reversals and excursions are present.

Table 1
Parameters values of the numerical experiments

Number of levels	L	15
Parameters of coupling	α_0	10^{-2} year^{-1}
	γ_0	10^{-3} year^{-1}
Parameter of relaxing	D_0	10^{-2} year^{-1}
Parameter of annihilation	S_0	0.05 year^{-1}
Parameter of disintegration	β_0	10^{-2} year^{-1}
Parameter of turbulence	E_0	10^{-3} year^{-1}
Efficiency of the direct cascade	F_0	4 year^{-1}
Scaling parameter (q)		1.5
Scaling parameters (δ, σ, b_0, ε, g, μ)		0.9
Parameters of retroaction	λ	10^{-9} nT^{-2}
	κ	10^{-9} nT^{-2}
	ν	10^{-10} nT^{-2}
Parameters of the differential equations	K_S, K_T	10^{-4} year^{-1}
	ζ_T	3×10^{-3} yr^{-1}
	ω	2×10^{-4} yr^{-1}

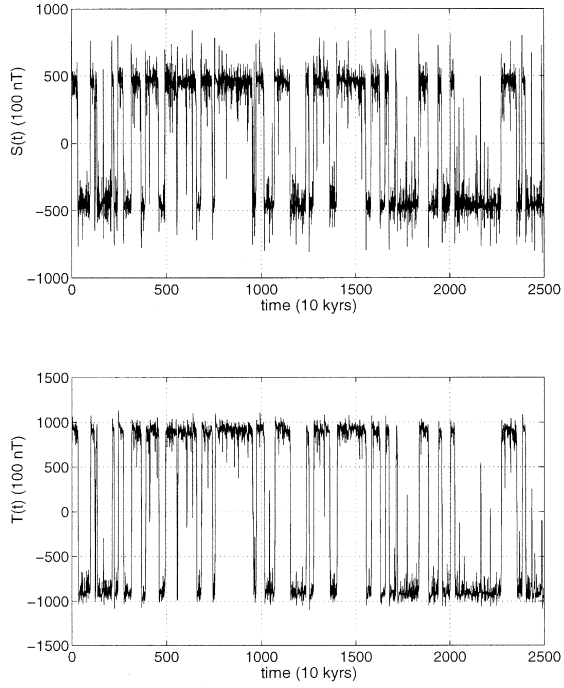

Fig. 3. (top) Evolution of $S(t)$ vs. time. (bottom) Evolution of $T(t)$ vs. time.

The duration of the chrons is varying, but is always much longer than the duration of the reversals, which is of the order of a few thousands of years. The distribution of the chrons durations for a 2×10^2 Ma long time interval is illustrated by the two graphs of Fig. 4; these graphs are comparable with the ones corresponding to the true geomagnetic field over the last 2.5×10^2 Ma (Merrill et al., 1996; but see Section 7). Fig. 5 gives another presentation of the succession of polarity intervals, which is classical in paleomagnetism and geodynamics. A phase diagram, in the form of a graph representing the $(S(t), T(t))$ points, is given in Fig. 6.

Before commenting on these figures, let us summarily explain how the model works.

5.1. How the model generates a large magnetic field from a stray field

Let us suppose that, at time $t = t_0$, $S(0) = \epsilon$, $T(0) = \epsilon'$, ϵ, ϵ' being small compared to S_0 and T_0 (the values reached by the field during polarity inter-

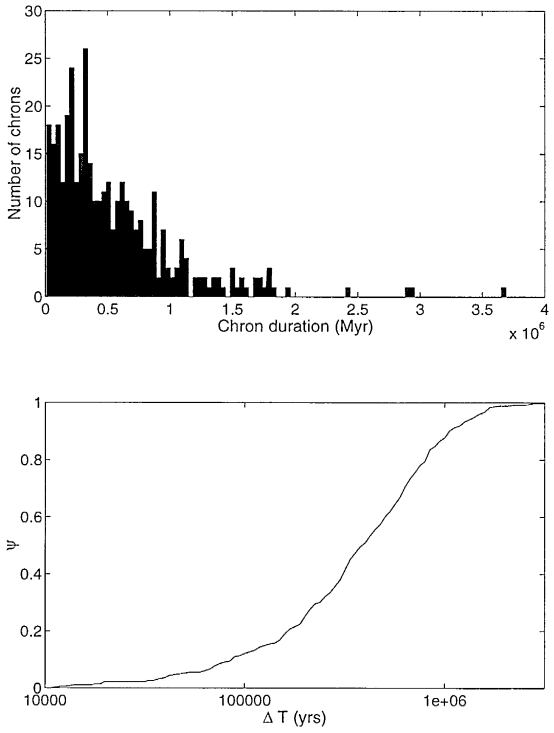

Fig. 4. (top) Histogram of the chrons durations; (bottom) cumulative density of chrons ψ as a function of their duration ΔT (in logarithmic scale); chrons shorter than 10^4 years are not considered.

vals), and $p_1^+(l,0) = p_1^-(l,0) = p_2^+(l,0) = p_2^-(l,0) = 0\ \forall l$, and let us start our system (Eqs. 4 and 5). Thanks to the regular appearance of new cyclones generated by the turbulence (E_0 in Eq. (6)), cyclones start occupying the vacant cells. As long as S and T are small, Δp (Eq. (15)) is highly fluctuating around zero (Δp is then, since the reaction of the magnetic field is weak, nothing else than $H(t)$ of (II); see Fig. 7 and Figs. 9–12 of (II)). Now, as said previously, if $\Delta p\omega > 0$, both S and T increase in magnitude keeping the same sign ($ST > 0$); due to the fluctuations of $(p_1(l) - p_2(l))$, especially at small scales, this situation always happens. As S and T increase, the coupling of [+] cyclones with the same orientation gets more and more efficient (Eq. (11)); cyclones of orientation 1 predominate in this phase of field increasing; the magnetic fields increase all the more until the density of 1[+] cyclones of higher levels gets close to unity. The saturation mechanism (Eq. (14)), which is more and more efficient when the fields increase, acts then in such a way as to fill the highest levels cells with [−] cyclones, predominantly of 1 orientation; the increase of the magnetic fields is stopped (Eq. (15)). At the same time, the disintegration of [−] cyclones, which generates the direct cascade, very active during the phase of building up of the fields, is slowed by these fields when they get large intensities. A situation is then reached where $(p_1(l) - p_2(l)) > 0\ \forall l$, with a predominance of [−] cyclones (the stronger this predominance is the larger the level is (see Eqs. 11–13), and S and T take their saturation values, characteristic of the field intensities during chrons. Let us stress that the mechanism always leads to large amplitude fields whatever is the initial distribution of $p_i^{\pm}$.

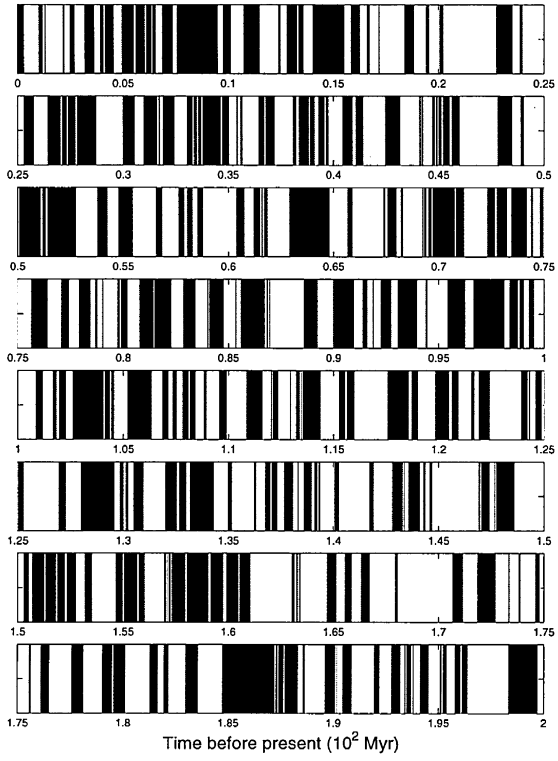

Fig. 5. Geomagnetic polarity time scale corresponding to $S(t)$ of Fig. 3 over 2×10^8 years. Chrons shorter than 10^4 years are not considered.

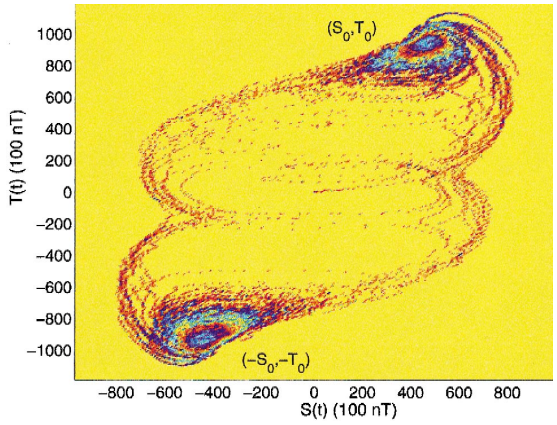

Fig. 6. Phase diagram $(S(t),T(t))$ corresponding to Fig. 3: the density of spots is an indicator of the temporal concentration and points out the values of the average values S_0, T_0 during the chrons.

5.2. Behaviour of the model during a polarity interval and route to inversions

Let us see how the model will evolve starting from the state reached — say at time t_1 — in the first step we have just described, and that we will call state I. State I is quite stable, essentially because the disappearance of $1[-]$ cyclones at all scales results, through the direct cascade, in maintaining $(p_1(l) - p_2(l)) > 0$ at smaller scales. In fact, a long preparation to a reversal or an excursion is required (we mean long — on the average — compared to time $(t_1 - t_0)$ needed to complete the first step leading to state I). Basically, 1 cyclones have to be replaced by 2 cyclones at all scales. This is illustrated in Fig. 8, which shows the evolution of the parameter $\xi = \sum_{l=1}^{L}(p_1^-(l) - p_2^-(l))$. From t_1 (and similar moments of time), ξ decreases more or less regularly, until some time before the next event, it plunges to negative values. During the reversal, or the excursion, this parameter recovers a high positive value due to the mechanism already described, which leads to state I. It is to be noted that the evolution to an excursion is the same as to a reversal. Some excursions can be preceded by a moderately low value of ξ. Smaller values can announce either an excursion or a reversal; in this case, it is a matter of chance that the new state I reached after an event has one polarity or the other. The unstable state reached at small magnetic fields intensities has no memory of the previous history and can lead to a reversal or an excursion.

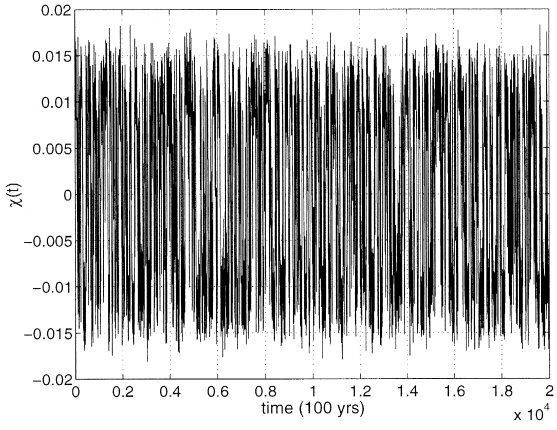

Fig. 7. Evolution of Δp without retroaction (or with $S = T = 0$). Δp strongly fluctuates. These large fluctuations favor the building up of the magnetic fields (see Section 5.1) when S and T are weak.

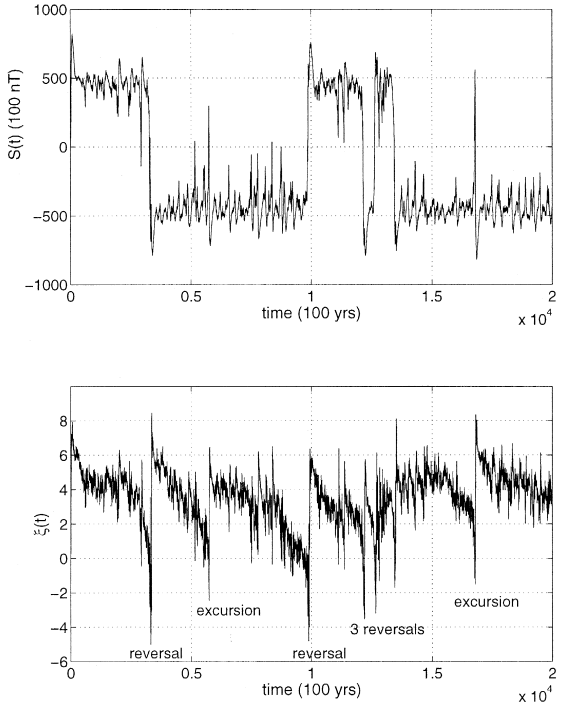

Fig. 8. (top) Evolution of $S(t)$ vs. time in a subinterval of Fig. 3. (bottom) Evolution of $\xi(t)$ vs. time during the same time span.

Parameter ξ is a global parameter, over all the scales. The behaviour of $(p_1^-(l) - p_2^-(l))$ scale by scale is illustrated in Fig. 9 (the number of levels, L, is taken small here, equal to 10, for illustration; the behaviour of the model is remarkably independent of the value of L). Although the graphs are rather complex, some clear features emerge. First, the time constant of the fluctuations of $p^-(l)$ increases with l. At short scales, the time spans over which $p_2^- > p_1^- > 0$ are short and unequally distributed, although their average frequency tends to be inversely proportionnal to the duration of the current chron divided by the number of cells of level l. At intermediate scales, typical features appear in the form of almost symmetrical — with respect to 0.5 — variations of p_1^- and p_2^- forming a sequence of triangle-shape patterns. p_1 decreases from values close to unity to values close to 0.5, whereas p_2 increases from small values up to values close to 0.5; and the two curves often intersect. Characteristic features are associated with the events (inversions and excursions), which appear as vertical bars on the graphs; a zoom of these bars shows that $p_1^- - p_2^- \sim 0\ \forall l$, just before the event, becomes strongly negative in the first part of the event and recovers a strong positive value at the end of the event (see caption of Fig. 9).

What makes the model rich is the permanent exchanges between the different levels. It is not easy to understand them in detail, and we will limit ourselves to a sketchy description. Let us, for illustration, isolate the exchanges between the lowest level $l = 1$ and the immediate higher level $l = 2$. Consider a time interval where at $l = 1$, $p_1^- - p_2^- < 0$; as $[-]$ cyclones come from $[+]$ ones, it means that

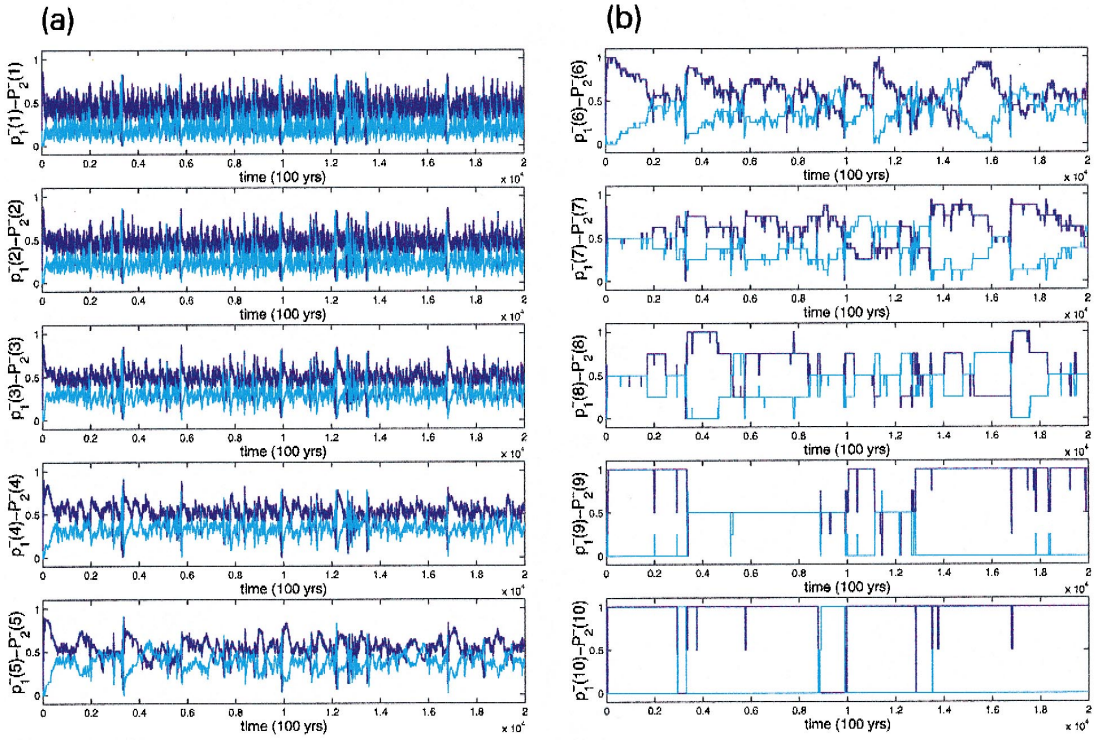

Fig. 9. For the fields shown in Fig. 8: (a) from top to bottom evolution of $p_1^-(l,t)$ and $p_2^-(l,t)$, $l \in [1,5]$, vs. time; (b) from top to bottom evolution of $p_1^-(l,t)$ and $p_2^-(l,t)$, $l \in [6,10]$, vs. time. We see that the two first reversals are due to the disappearance of 2 orientations cyclones at the highest level ($l = 10$). The appaearance of these cyclones is due to the exchanges process between 1 and 2 cyclones at all scales (with a time scale increasing with l). For the next event, this process does not take place at the highest scale : for the three consecutive reversals the fluctuations at scale $l = 6$ are important while for the last excursion we observe the disappearance of 2 cyclones at scale $l = 8$.

2[+] cyclones dominated on 1[+] cyclones some time before (the relaxation time). This predominance of 2[+] at $l = 1$ will induce a statistical increase of 2 cyclones (first 2[+] and, after the relaxation time, 2[−]) at $l = 2$ through the inverse cascade mechanism: during these time intervals of 2[+] dominance at $l = 1$, the fields S and T become weaker (see Eq. (15)); the direct cascade is made more effective (Eq. (13)) and concerns mostly 1 cyclones, which are dominant at $l = 2$ (recall that we start from state I); cells are made vacant at $l = 2$, which will be occupied dominantly by 2 cyclones due to the coupling of cyclones of level 1, since 2 cyclones dominate at $l = 1$ (the coupling mechanism keeps active despite the small reduction of the field intensities). As a result a certain number of 2 cyclones will have replaced 1 cyclones at $l = 2$ (inverse cascade) while 1 cyclones will dominate again at $l = 1$ (direct cascade). The same can be said about the exchanges between level l and level $l + 1$ (in fact, all the exchanges processes take place simultaneously). The mechanism just described, repeated a number of times, leads to a progressive balance of 1[−] cyclones and 2[−] cyclones at all the scales (whence the form of the graph of Fig. 9). As a global result, the parameter ξ decreases (Fig. 8(b)) . As long as ξ keeps high enough positive values, the probability that 2 cyclones dominate 1 cyclones at the highest levels is negligible. We are in the domain of the secular variation (S.V.; Section 1), i.e. of the fluctuations of S and T between the events, where the system keeps a memory of its previous state polarity. When the process just described leading to an approximate balance of 1 and 2 at all levels is practically completed, and $\xi \sim 0$, this probability (that 2 cyclones dominate 1 cyclones at the highest levels) becomes high and the system is ready for an event: a time interval where 2[+] cyclones are predominant at the lowest level makes — as above — the direct cascade more effective, but, now, it involves mostly 2 cyclones. Both direct and inverse cascades are dominantly cascades of 2 cyclones, 2 cyclones dominate at all scales, and this accelerates the decrease of the fields. S and T become small. As said in Section 5.1, Δp highly fluctuates around zero. In this unstable state, the system loses all memory of the state it occupied before the start of the event; the process of field regeneration acts again, as described in Section 5.1, to produce a reversal (change of polarity) or an excursion (return to the same polarity).

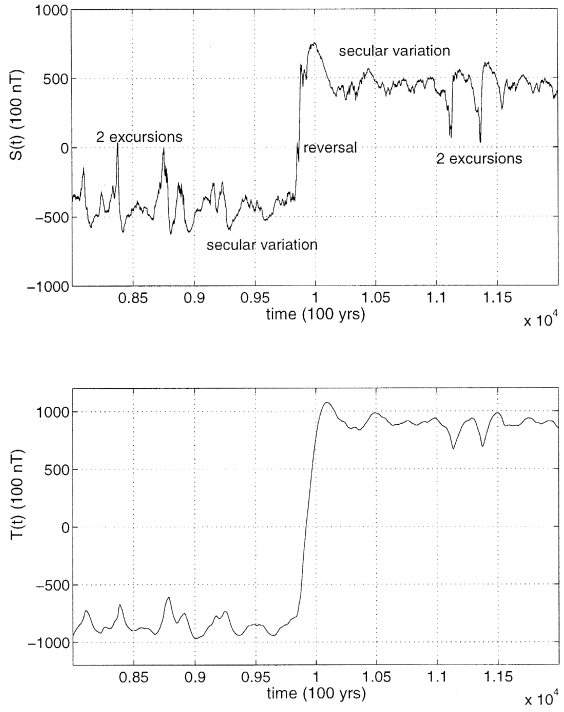

Fig. 10. Around a reversal: (top) evolution of $S(t)$ vs. time; note the short oscillations around 0 during the reversal. (bottom) Evolution of $T(t)$ vs. time.

Let us stress that, due to the mechanism of exchange of orientations described above, reversals always occur; more precisely, however long we run the model, no chron happens to exceed 5 Ma. Note that there is no clear cut boundary between the largest fluctuations of the S.V., excursions and reversals (for fields fluctuations all the range of magnitudes is observed).

Fig. 10 is a zoom of the part of the recordings of S and T in the neighbourhood of the reversal occurring around $t = 1$ Ma ($t = 0$ is the beginning of the numerical experiment).

6. The α^2 model

We will now present more briefly, as announced in Section 1, the α^2 model.

6.1. Schematic equations of a α^2 dynamo

As in the case of classical α^2 dynamos Steenbeck and Krause, 1969; Roberts, 1972, the source term of toroidal field, symmetric of the source term of poloidal field, results from the interaction of the turbulent helical flow with the poloidal field. The equations of our α^2 dynamo then write:

$$\frac{\partial T}{\partial t} + K_T T = \Delta p \zeta_T S, \tag{16}$$

$$\frac{\partial S}{\partial t} + K_S S = \Delta p \zeta_S T. \tag{17}$$

The symmetry of the system is changed with respect to the system of Eqs. 4 and 5. In the case of the $\alpha\omega$ model, polarity intervals of both signs are associated with a predominance of 1 cyclones while a predominance of 2 cyclones must take place for the fields to be destabilized (for ω and $\zeta_T > 0$), whichever their signs are and an event — excursion or reversal — to occur. But here, 1 cyclones dominate during the chrons where $ST > 0$, and 2 cyclones during the chrons where $ST < 0$ (for ζ_S and $\zeta_T > 0$). In fact, $T(t)$ keeps a constant sign all the time in the present realisation; only S changes its sign. In the first case, 2 cyclones must happen to dominate (in the sense discussed in Section 5.1) to trigger an event; in the second case, 1 cyclones must happen to dominate.

Remark: There is no reason to suppose that the turbulence is inefficient to generate a toroidal field. In $\alpha\omega$ model, it is just supposed that the ω effect — differential rotation — is more efficient. That means $\omega \gg \zeta_T \Delta \bar{p}$ in Eqs. 4 and 5 ($\Delta \bar{p}$ for the mean value of Δp) and leads to a strong field dynamo in which $|T| \gg |S|$. In the chosen example, we took only $\omega \sim 2\zeta_T \Delta \bar{p}$ as a first step towards a strong field dynamo.

6.2. Realisations of an α^2 dynamo

Fig. 11 illustrates a realisation of the α^2 model for the values of parameters given in Table 1 except for $K_S = 2 \times 10^{-4}$, $\zeta_S = \zeta_T = 1.5 \times 10^{-3}$. Fig. 11 represents the evolution of $S(t)$ and $T(t)$ over a time span of 3×10^6 time steps (the time step is still here approximately 1 year). As in the case of Fig. 3,

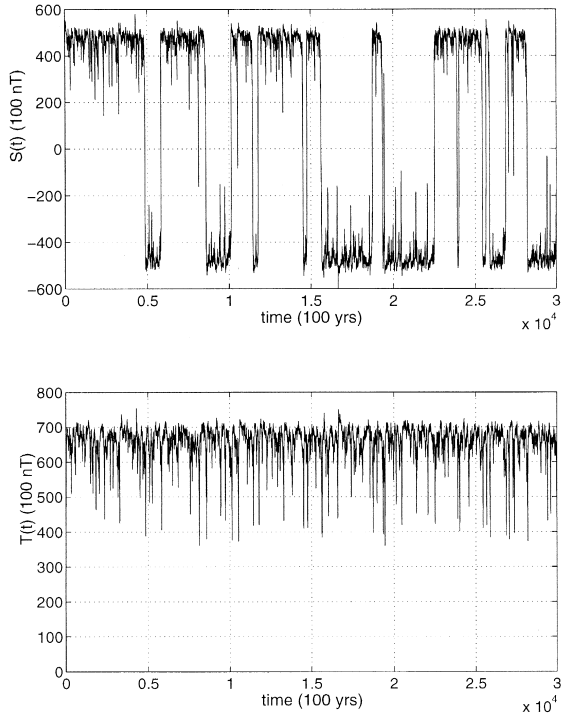

Fig. 11. α^2 dynamo. (top) Evolution of $S(t)$ vs. time; (bottom) evolution of $T(t)$ vs. time.

polarity intervals (chrons), excursions, reversals and S.V. are present on the graph of the poloidal field $S(t)$. $T(t)$ does not reverse; events on S are marked by sharp changes on T, but not significantly larger than the changes corresponding to regular S.V. Fig. 12 shows the evolution of $\xi(t)$ — with the same definition as in Section 5.2 — for the same time period.

Let us briefly explain how the model works; much of what was said in the case of the first model can be resumed, mutatis mutandis. The building of a large field from a stray field, starting again at time $t = 0$ with $p_1^+(l,0) = p_1^-(l,0) = p_2^+(l,0) = p_2^-(l,0) = 0\ \forall l$, can be understood as in the $\alpha\omega$ case. But here, the large field state, which is reached at time t_1 — the starting time of the chron — has $ST > 0$ or $ST < 0$ according to which orientation of cyclones 1 or 2 happens to first dominate, enough to launch the building process. The state (S_0, T_0) is quite stable ($S_0 > 0$ or $S_0 < 0$). It will not be destabilized before a somewhat continuous erosion of the predominance of 1 cyclones ($ST > 0$) or 2 cyclones ($ST < 0$) has

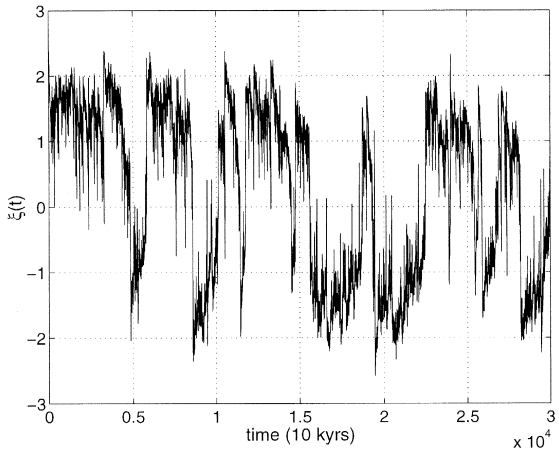

Fig. 12. Evolution of ξ vs. time corresponding to the fields shown in Fig. 11.

taken place. This phenomenon appears again clearly on the graph of the global parameter ξ (Fig. 12) whose sign is correlated with the sign of S; ξ presents a decreasing trend — on which strong fluctuations are superimposed — before the next event occurs. Note however that, as in the $\alpha\omega$ case, the duration of the preparation process is random and that, consequently, a large interval of chrons durations is observed. We will come back to this feature in the discussion.

Let us now have a look at what happens scale by scale and at the exchanges between scales. For this illustration L is taken again equal to 10; Fig. 13 displays the graphs of $p_1^-(l)$ and $p_2^-(l)$. The pattern at low intermediate scales ($l \leq 5$) appears quite simple: 1 cyclones largely dominate when $S_0 > 0$, 2 cyclones largely dominate when $S_0 < 0$; variations of p_1 and p_2 tend to be symmetrical with respect to a value ~ 0.5. Passages from a polarity to the other are sharp at the scale of the graph. At higher intermediate scales ($l \geq 6$), the pattern shows, although less clearly than on the global parameter ξ graph, a decrease of the number of dominant orientation cy-

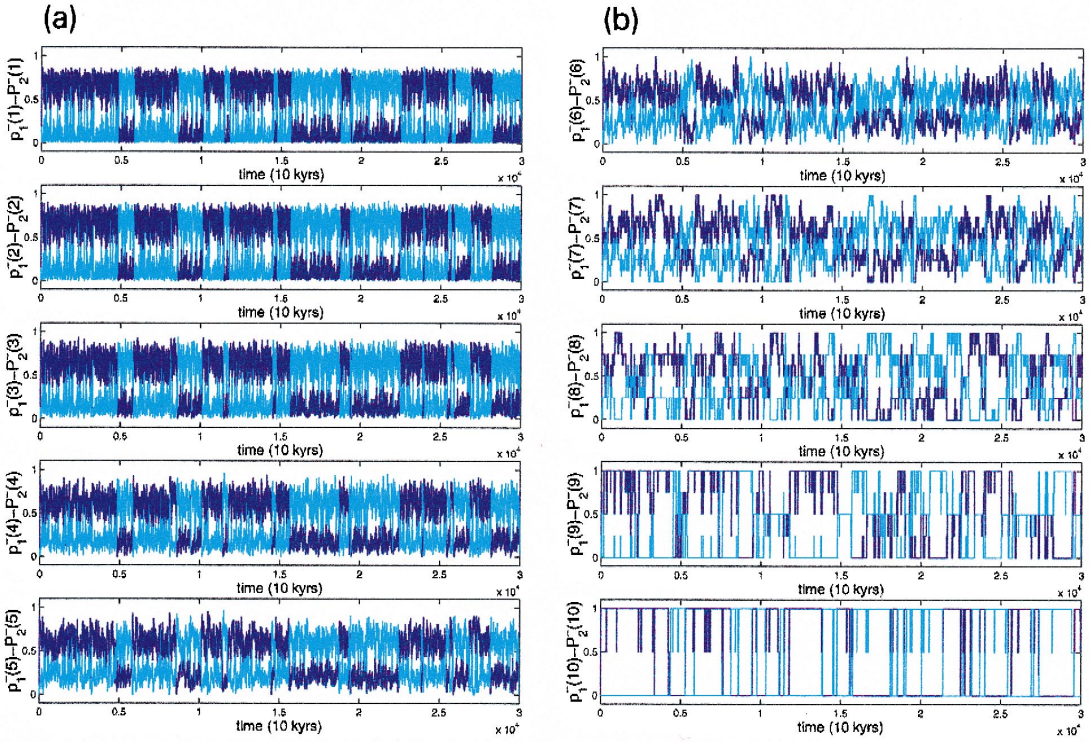

Fig. 13. (a) From top to bottom: evolution of $p_1^-(l,t)$ and $p_2^-(l,t)$, $l \in [1,5]$, vs. time; (b) from top to bottom: evolution of $p_1^-(l,t)$ and $p_2^-(l,t)$, $l \in [6,10]$, vs. time.

clones before an event. At the highest scales, the graphs are more difficult to read due to the weak number of cyclones involved. The transfer of helicity from scale to scale can again be understood as in the case of the first model, although here each orientation (1 or 2) is associated with one polarity of the field $S(t)$.

Remark: In the present realisation, $T(t)$ does not reverse, but for other sets of values of parameters, both $S(t)$ and $T(t)$ reverse.

7. Discussion

The model consisting of the system of equations (Eqs. 4 and 5, or Eqs. 16 and 17), together with the multiscale turbulent motion leading to the computation of $\Delta p\zeta_T$ (or $\Delta p\zeta_S$ and $\Delta p\zeta_T$), gives — for a wide range of values of the parameters — a behavior reproducing satisfactorily the behavior of the dipolar geomagnetic field over geological times. Polarity intervals, excursions, reversals are observed. The duration of the events (excursions and reversals) is short compared with the duration of the polarity intervals (chrons). The distribution of the chrons lengths provided by the model follows an exponential law in an interval of durations comparable with the corresponding interval for the real field when choosing properly the time unit (however, some features of the actual paleomagnetic field are not recovered, as discussed below).

The present model being some combination of the models of papers (I) and (II), its behaviour borrows features from both of them, but also presents differences with respect to both of them. Part of the global structure of (I) is conserved, but no a priori lack of symmetry (of orientations 1 and 2) is introduced in the model, the duration of the events is shorter, and their mechanisms different, the secular variation is much stronger and more irregular. Differences with respect to model (II) were of course expected since what was the secondary magnetic field itself generated by the dynamo mechanism in (I) is now a source term in the r.h.s. of the differential (Eqs. 4, 5, 16 and 17), and since a retroaction of the magnetic field on the flow has been introduced. As a result, the way the polarity intervals are maintained and the events occur are significantly different. In (II), $H(t)$ itself presented spontaneous long lived symmetry breakings, and the periods of symmetry breaking were simply the chrons. Here, strong values of $\Delta p\zeta_{S,T}$ are needed during the events, i.e. large $|\sum_l p^+(l) - p_2^2(l)|$. During the polarity intervals, much smaller values of $\Delta p\zeta_{S,T}$ are needed, just enough to balance diffusion. Fig. 14 illustrates this situation. This behaviour of $\Delta p(t)\zeta_{S,T}$ which, roughly speaking, looks like $\dot{H}(t)$ of (II) is expected (recall that $\Delta p\zeta_T T$ or $\Delta p\zeta_S S$ are source terms in the r.h.s. of differential equations) and comes from the rather rapid transformation of [+] cyclones into [−] (less efficient) cyclones, and also from the reaction of the magnetic field on the helical motion.

Another difference from (II) and an important feature of the present model is that during chrons, the destabilization of the field cannot occur from a large fluctuation of the injected turbulence by itself (Eq. (6)). The preparation process described above (see Section 5.2) is necessary and is still obtained with small-scale turbulence only (for example if Eq. (6) becomes $T(l) = E_0\,\delta(l-1)$ with δ as the Dirac function).

We do not present realisations corresponding to a range of parameters values. In fact, the series produced by the model do not depend strongly on the parameters values except for the average duration of the chron; for example, if we add larger scales (increase the value of L), the average duration becomes larger (this is not the case if we add smaller

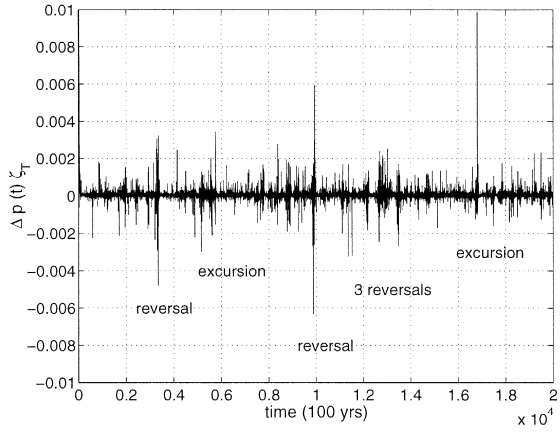

Fig. 14. Evolution of $\Delta p\zeta_T$ vs. time corresponding to the fields shown on Fig. 8(a).

ones, keeping the same parameters for the highest level).

As discussed in Sections 5 and 6, reversals and excursions are prepared by a slow (compared to events duration) erosion of the number of cyclones favourable to the current polarity of the field (cyclones with the orientation in agreement with the sign of ω in case of an $\alpha\omega$ dynamo, with the orientation corresponding to one or the other polarity in case of an α^2 dynamo) to the benefit of the other orientation cyclones. In a sense, the changes of polarity of the magnetic field are less spontaneous than in (II) (although the symmetry properties of the helical flow are conserved). There is in fact a correlation between the duration of the chron to come and the intensity of the symmetry breaking (characterized by ξ) just after the event. Fig. 15 shows the variation of $\langle \xi \rangle_1$, the average value of ξ over 50 ka after the values $(S_0;T_0)$ have been recovered, and the chron duration. ξ increases with the chron duration until it reaches a maximum value. The existence of such a predictive parameter — although only in a statistical sense — is a characteristic feature of the model. Is there any indication of this preparation process in paleomagnetic data? Valet and Meynadier (1993) have given evidence of a saw-teeth evolution of the intensity of the paleomagnetic field (Fig. 1): its intensity is smaller — in most cases — before a reversal, it is larger just after it, at the onset of a new chron. In fact, there is a strong similarity between the graph of Fig. 1 and the one of Fig. 8 representing $\xi(t)$. The preparation process is not directly apparent on the graphs of $S(t)$, but could be made so, through a light modification of the algorithm (see Section 8). The question whether the core flow changes slowly its configuration during a chron, preparing the next event, or if an event occurs as a sudden instability without any qualitative change in the motion before it, is an open question. Valet and Meynadier's results seem to favour the first scenario. It is fair to mention that the changes in the intensity of the field reported by these authors are not considered as genuine by all the paleomagneticians (McFadden and Merrill, 1997; Coe, 1993).

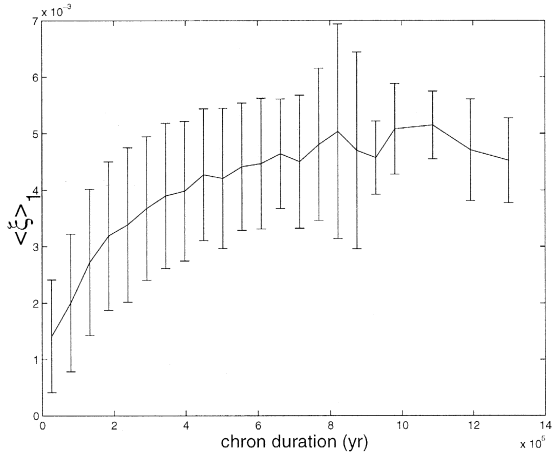

Fig. 15. Average value of ξ during 50 ka $\langle \xi \rangle_1$ after a reversal vs. the duration of the chron to come; the standard deviation of $\langle \xi \rangle_1$ is represented by a vertical bar. The sequence includes 6×10^3 chrons giving the histogram of Fig. 4.

During an event, in the state where the fields $S(t)$ and $T(t)$ are weak (Section 5.1), the system loses all memory of its previous history. It can evolve to either polarity of the field, independently of the polarity, which prevailed before the starting of the event. This is in sharp contrast with the behaviour of the system during the chrons where it presents the slow continuous evolution described above.

As already mentioned, the histogram of the chrons duration of the model can be made to fit the corresponding histogram for the paleomagnetic field if one keeps only durations larger than 10 ka as it is usual with paleomagnetic data. But of course, we can here consider much shorter durations; the complete histogram in a logarithmic scale is illustrated in Fig. 16(a). The histogram is clearly three-modal. Now if, again in function of the chron duration, we represent $\langle \xi \rangle_2$, the mean value of ξ over the whole duration of this chron, we get Fig. 16(b) for the same realisation of the model as used for Fig. 16(a). The right subset of points $(\langle \xi \rangle_2, \Delta T)$ (with $\langle \xi \rangle_2 > 0$ and $\Delta T >> 10^4$) corresponds to the polarity intervals, i.e. the stable states reached after an event. The central subset of points $(\langle \xi \rangle_2, \Delta T)$ (with $\langle \xi \rangle_2 < 0$ and $\Delta T < 10^4$) corresponds to the fluctuations during the events or to a pair of reversals less than 10 ka apart. The leftward subset of points $(\langle \xi \rangle_2, \Delta T)$ (with $\langle \xi \rangle_2$ centered around 0 and $\Delta T \ll 10^4$) corresponds to the short excursions (which could also be called large S.V. oscillations). A gap is observed between the central and the right subsets of points. Durations around 20 ka are relatively rare; when the

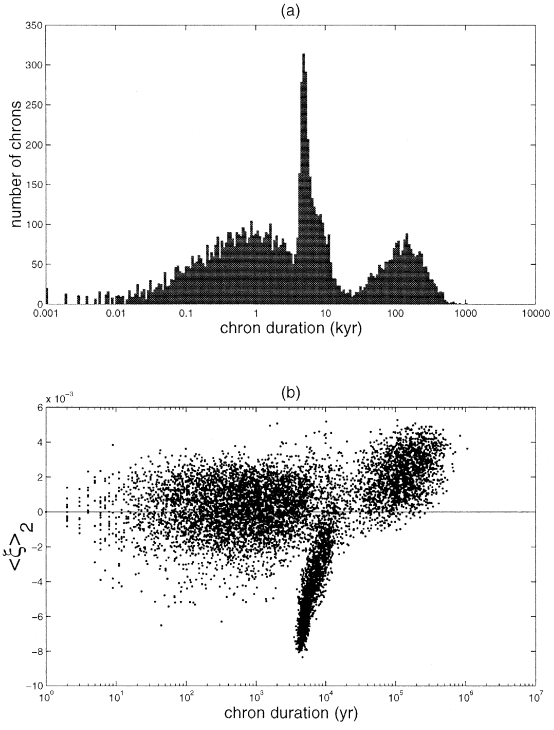

Fig. 16. (top) Histogram of the chrons durations. (Bottom) Average value of ξ, $\langle \xi \rangle_2$, during a whole chron vs. the duration of this chron.

fields have been established, it takes some time to destabilize them. This might be drawn nearer to an observation of McFadden and Merrill (1993).

Despite a similar trend in the chrons durations distributions, the model does not display, as the geomagnetic field does, superchrons, nor any evolution with time of the average reversals frequency (as seen from running the model for very long times). This is of course expected. Superchrons of the magnetic field appear as rare events. Special conditions in the core or at the core–mantle boundary (CMB), although vaguely stated (e.g. Gallet and Hulot (1997)), are supposed to exist when they occur in the history of the geomagnetic field. The observed trend in the reversals frequency observed over the last 100 Ma (e.g. Gallet and Courtillot (1995)) is also attributed to changes at the CMB (Glatzmaier et al., 1999). The parameters of our model do not vary with time; it would of course be easy to introduce such a time variation to simulate time changes in some boundary condition or forcing mechanism. But more interesting, a rather light modification of the model can lead to superchrons (Narteau et al., in preparation) and possibly also to a very long time constant in the S and T time variation, i.e. in the average events frequency. The question whether it is necessary or not to modify the system — boundary conditions or forcing — to get rare situations like superchrons, or a long time constant trend of the reversals frequency, is of high geodynamical interest. As mentioned in the Introduction, the question of changing boundary conditions is also raised by Hide (1998).

8. Perspectives and conclusion

The present model is an attempt to bring the multiscale helical flow of (II) into a scheme — however abstract and oversimplified — of an autoexcited dynamo. The helical turbulence model, with its two cascades, direct and inverse, displays constant and complex exchanges between the scale levels, with both slow time constants and sudden instabilities. Such a system, with its constant and vivid interactions between eddies of different scales, is prone to produce time series looking alike the recordings of the paleomagnetic field.

We are of course aware of the schematic characteristics of the model, notably through the introduction of a single poloidal and a single toroidal modes. Interactions between all scales of motion and all scales of magnetic field are ignored; one could bring forward the high value of the Prandtl magnetic number, the ratio of magnetic diffusivity to kinematic viscosity ($\sim 10^{-6}$) in the core fluid. Retrieving features observed in the behavior of the paleomagnetic field cannot be considered as a proof of the model validity. At least, it permits to discuss in a novel way the succession of chrons and reversals. Further developments in several directions can be envisioned (and started). Space coordinates and geometry can be introduced by coupling a stochastic time dependent model with the formalism of the multiscale motion (as we recently did with the SOFT model of earthquake generation, Narteau et al., 2000); another way toward the same objective is to consider several domains in the fluid and couple them by various interactions, which will allow to consider several modes of the field (the two procedures being remi-

niscent of respectively real space and spectral techniques). Another investigation will bear on a better formalisation of the interactions and feedback mechanisms. To conclude, let us say that the kind of reasoning and formalism used in the present paper can be viewed as pertaining to a vast current of nonlinear methods in physics and geophysics in which it is possible to find similar cases and ideas of further developments.

Acknowledgements

E. Blanter and M. Shirman were partially supported from IPGP and National Sciences Foundation Grant EAR-9804859 and INTAS grant 93-809-ext.

References

Backus, G., 1958. A class of self-sustaining dissipative spherical dynamos. Am. Phys. 4, 543–585.

Blanter, E., Narteau, C., Shnirman, M., Le Mouël, J., 1999. Up and down cascade in a dynamo model: spontaneous symmetry breaking. Phys. Rev. E 59, 5112–5123.

Braginsky, S., 1978. Nearly axially symmetric model of the hydrodynamic dynamo of the earth. Geomagn. Aeron. 8, 225–231.

Braginsky, S., Roberts, P., 1987. A model geodynamo. Geophys. Astrophys. Fluid Dyn. 38, 327–349.

Brito, D., Cardin, P., Nataf, H., Marolleau, G., 1995. Experimental study of a geostrophic vortex of gallium in a transverse magnetic field. Phys. Earth Planet. Inter. 91, 77–98.

Bullard, E., Gellman, H., 1954. Homogeneous dynamosand terrestrial magnetism. Philos. Trans. R. Soc. 247, 213–278.

Cardin, P., Olson, P., 1995. The influence of toroidal magnetic field on thermal convection in the core. Earth Planet. Sci. Lett. 132, 167–181.

Chandrasekar, S., 1961. Hydrodynamic and Hydromagnetic Stability. Clarendon Press, Oxford.

Coe, R., 1993. A swifty changing field. Nature 366, 205–206.

Frisch, U., Léorat, J., Mazure, A., Pouquet, A., 1975. Possibility of an inverse cascade in MHD helical turbulence. Fluid Mech. 68, 769–778.

Gallet, Y., Courtillot, V., 1995. Geomagnetic reversal behavior since 100 Ma. Phys. Earth Planet. Inter. 92, 235–244.

Gallet, Y., Hulot, G., 1997. Stationary and nonstationary behavior within the geomagnetic polarity time scale. Geophys. Res. Lett. 24, 1875–1878.

Glatzmaier, G., Coe, R., Hongre, L., Roberts, P., 1999. The role of the Earth's mantle in controlling the frequency of geomagnetic reversals. Nature 401, 885–890.

Glatzmaier, G., Roberts, P., 1995a. A three-dimensional convective dynamo solution with rotating and finitely conducting inner core and mantle. Phys. Earth Planet. Inter. 91, 63–75.

Glatzmaier, G., Roberts, P., 1995b. A three-dimensional self-consistent computer simulation of a geomagnetic field reversal. Nature 377, 203–209.

Gubbins, D., 1974. Theories of the geomagnetic and solar dynamos. Rev. Geophys. Space Phys. 12, 137–154.

Hide, R., 1998. Nonlinear quenching of current fluctuations in a self-exciting homopolar dynamo. Nonlinear Proc. Geophys. 4, 201–205.

Kageyama, A., Sato, T., 1997. Generation mechanism of a dipole field by a magnetohydrodynamic dynamo. Phys. Rev. E 55, 4617–4626.

Krause, F., Rädler, K.-H., 1980. Mean-Field, Magnetohydrodynamics and Dynamo Theory. Pergamon.

Kuang, W., Bloxham, J., 1997. An earth-like numerical dynamo model. Nature 389, 371–374.

LeMouël, J., Allègre, C., Narteau, C., 1997. Multiple scale dynamo. Proc. Natl. Acad. Sci. U. S. A. 94, 5510–5514.

McFadden, P., Merrill, R., 1993. Inhibition and geomagnetic field reversals. J. Geophys. Res. 98, 6189–6199.

McFadden, P., Merrill, R., 1997. Sawtooth paleointensity and reversals of the geomagnetic field. Phys. Earth Planet. Inter. 103, 247–252.

Meneguzzi, M., Frisch, U., Pouquet, A., 1981. Helical and non helical turbulent dynamos. Phys. Rev. Lett. 47, 769–778.

Merrill, R.T., McElhinny, M.W., McFadden, P.L., 1996. The Magnetic Field of the Earth. Academic Press.

Moffatt, H.K., 1978. Magnetic Field Generation in Electrically Conducting Fluids. Cambridge Univ. Press.

Narteau, C., Shebalin, P., Holschneider, M., LeMouël, J.L., Allègre, C.J., 2000. Direct simulation of the stress redistribution in the scaling organization of fracture tectonics. G.J.I. 141, 115–135.

Nozières, P., 1978. Reversals of the earth's magnetic field; an attempt at a relaxation model. Phys. Earth Planet. Inter. 174, 55–74.

Pouquet, A., Patterson, G., 1978. Numerical simulation of helical magnetohydrodynamic turbulence. Fluid Mech. 85, 305–323.

Rikitake, T., 1958. Oscillations of a system of disk dynamos. Proc. Cambridge Philos. Soc. 54, 89–105.

Roberts, P., 1971. Dynamo theory: mathematical problems in the geophysical sciences. In: Lectures in Applied Mathematics vol. 14 A.M.S Providence, Rhode Island, pp. 129–205.

Roberts, P., 1972. Kinematic dynamo models. Philos. Trans. R. Soc. 277, 287–315.

Steenbeck, M., Krause, F., 1969. On the dynamo theory of stellar and planetary magnetic fields. Astron. Nachr. 291, 271–286.

Valet, J., Meynadier, L., 1993. Geomagnetic field intensity and reversals during the past four million year. Nature 366, 234–238.